Multi-shell effective interactions

Naofumi Tsunoda
Department of Physics, The University of Tokyo, 7-3-1 Hongo, Bunkyo-ku, Tokyo, Japan

Kazuo Takayanagi
Department of Physics, Sophia University, 7-1 Kioi-cho, Chiyoda-ku, Tokyo 102, Japan

Morten Hjorth-Jensen
Department of Physics and Center of Mathematics for Applications, University of Oslo, N-0316 Oslo, Norway and National Superconducting Cyclotron Laboratory and Department of Physics and Astronomy, Michigan State University, East Lansing, Michigan 48824, USA

Takaharu Otsuka
Department of Physics and Center for Nuclear Study, The University of Tokyo, 7-3-1 Hongo, Bunkyo-ku, Tokyo, Japan and National Superconducting Cyclotron Laboratory and Department of Physics and Astronomy, Michigan State University, East Lansing, Michigan 48824, USA

(Received 25 October 2013; published 24 February 2014)

Background: Effective interactions, either derived from microscopic theories or based on fitting selected properties of nuclei in specific mass regions, are widely used inputs to shell-model studies of nuclei. The commonly used unperturbed basis functions are given by the harmonic oscillator. Until recently, most shell-model calculations have been confined to a single oscillator shell like the sd shell or the pf shell. Recent interest in nuclei away from the stability line requires, however, larger shell-model spaces. Because the derivation of microscopic effective interactions has been limited to degenerate models spaces, there are both conceptual and practical limits to present shell-model calculations that utilize such interactions.
Purpose: The aim of this work is to present a novel microscopic method to calculate effective nucleon-nucleon interactions for the nuclear shell model. Its main difference from existing theories is that it can be applied not only to degenerate model spaces but also to nondegenerate model spaces. This has important consequences, in particular for intershell matrix elements of effective interactions.
Methods: The formalism is presented in the form of a many-body perturbation theory based on the recently developed extended Kuo-Krenciglowa method. Our method enables us to microscopically construct effective interactions not only in one oscillator shell but also for several oscillator shells.
Results: We present numerical results using effective interactions within (i) a single oscillator shell (a so-called degenerate model space) like the sd shell or the pf shell and (ii) two major shells (nondegenerate model space) like the sdf_7p_3 shell or the pfg_9 shell. We also present energy levels of several nuclei that have two valence nucleons on top of a given closed-shell core.
Conclusions: Our results show that the present method works excellently in shell-model spaces that comprise several oscillator shells, as well as in a single oscillator shell. We show, in particular, that the microscopic intershell interactions are much more attractive than has been expected by degenerate perturbation theory. The consequences for shell-model studies are discussed.

DOI: 10.1103/PhysRevC.89.024313 PACS number(s): 21.30.Fe, 21.60.Cs

I. INTRODUCTION

The nuclear shell model, a sophisticated theory based on the configuration interaction method, has been one of the central theoretical tools for understanding a wealth of data from nuclear structure experiments. Owing to the rapid growth in the dimensionality of the Hilbert space with increasing degrees of freedom, we have to work within a reduced Hilbert space, the so-called model space. Accordingly, we use an effective interaction that is tailored to the chosen model space. This effective interaction forms an essential input to all shell-model studies. Equipped with modern sophisticated effective interactions, the shell model has successfully described many properties of nuclei.

There are two main approaches to determine effective interactions for the nuclear shell model. One is based on fitting two-body matrix elements to reproduce observed experimental data. This approach is widely used in nuclear structure studies and has been rather successful in reproducing properties of known nuclei and in predicting not-yet-measured properties of nuclei. The other approach is to *derive* the effective interaction using many-body theories, starting from bare nucleon-nucleon (NN) interactions.

Although the first approach has been widely used with great success [1–5], the main goal of effective interaction theory is to construct and understand such sophisticated effective interactions starting from the underlying nuclear forces and so-called *ab initio* or first-principles many-body

methods. Effective interactions in A-body systems have to be approximated, or else there would obviously be no need to obtain such an interaction. There is an extensive literature on various theoretical aspects and derivations of effective interactions. Most microscopic effective interactions, except for those used in no-core shell-model studies [6–8], are based on many-body perturbation theory, starting in many cases with the standard non-Hermitian Bloch-Brandow scheme [9–12] or with Hermitian effective Hamiltonians [13,14]. A standard approach to derive a microscopic effective interactions for the shell model is provided by many-body perturbation theory and the so-called folded-diagram [15] approach; see, for example, Ref. [16] for several implementations. Two widely used approaches are the Kuo-Krenciglowa (KK) [17] and the Lee-Suzuki (LS) [18] schemes. These approaches, however, are feasible only with degenerate perturbation theory and are thereby constrained to a model space consisting of typically one major oscillator shell. This poses a strong limitation on the applicability of the theory. Many unstable nuclei require at least two or more major oscillator shells for a proper theoretical description. For example, the physics of nuclei in the so-called island of inversion is currently explained with empirical effective interactions (see, for example, Ref. [3]) defined for a model space consisting of the sd shell and the pf shell. It is therefore absolutely necessary to establish a microscopic theory that allows us to construct an effective interaction for the model spaces composed of several oscillator shells, starting from realistic nuclear forces. Effective interactions defined for several shells can hopefully also ameliorate convergence issues related to many-body perturbation theory. In spite of several developments in many-body perturbation theory, there are still serious convergence issues, in particular when so-called intruder states are present; see Refs. [19,20] for an in-depth discussion.

Recently, the KK and the LS methods have been extended to the case of nondegenerate model spaces [21,22]. In this work, we present the extended KK (EKK) method in many-body systems, which allows us to construct a microscopic effective interaction for several shells. We see that our theory is a natural extension of the well-known folded-diagram theory of Kuo and his collaborators (see, for example, Refs. [15,17]).

This article is structured as follows. In Sec. II, we briefly explain the concept of the effective interaction in a given model space. In Secs. III and IV, we explain our EKK theory for effective interactions. We discuss in some detail the difference between the EKK method and the conventional KK approach, which applies to degenerate model spaces only. In Sec. V we present test calculations and discussions. Here we construct effective interactions for the nuclear shell model in a single major shell (sd shell, pf shell) and also in two major shells (sdf_7p_3 shell, pfg_9 shell). We then calculate energy levels of several nuclei that have two valence nucleons on top of a closed-shell core. We demonstrate that our method establishes one possible way to reliably compute microscopic effective interactions for model spaces composed of several major oscillator shells. In Sec. VI we give a brief conclusion and a summary.

II. EFFECTIVE INTERACTION IN MODEL SPACE

In this section we review briefly the formalism for deriving an effective interaction using many-body perturbation theory.

A. Model space

Suppose we describe a quantum system using the Hamiltonian

$$H = H_0 + V, \tag{1}$$

where H_0 is the unperturbed Hamiltonian and V is the perturbation. In a Hilbert space of dimension D, we can write the many-body Schrödinger equation as

$$H|\Psi_\lambda\rangle = E_\lambda|\Psi_\lambda\rangle, \quad \lambda = 1,\dots,D. \tag{2}$$

In shell-model calculations, however, the dimension D of the Hamiltonian matrix increases exponentially with the particle number, limiting thereby the applicability of direct diagonalization procedures to the solution to Eq. (2).

In this situation, we introduce a P space (model space) of a tractable dimension $d \leqslant D$ that is a subspace of the large Hilbert space of dimension D. Correspondingly, we define the projection operator P onto the P space and $Q = 1 - P$ onto its complement. We require that the projection operators P and Q commute with the unperturbed Hamiltonian H_0,

$$[P, H_0] = [Q, H_0] = 0. \tag{3}$$

B. Energy-dependent approach

We start our explanation by introducing an energy-dependent effective Hamiltonian. By use of the projection operators P and Q, we can express Eq. (2) in a partitioned form ($\lambda = 1,\dots,D$),

$$\begin{pmatrix} PHP & PVQ \\ QVP & QHQ \end{pmatrix}\begin{pmatrix} |\phi_\lambda\rangle \\ |\Psi_\lambda\rangle - |\phi_\lambda\rangle \end{pmatrix} = E_\lambda\begin{pmatrix} |\phi_\lambda\rangle \\ |\Psi_\lambda\rangle - |\phi_\lambda\rangle \end{pmatrix}, \tag{4}$$

where $|\phi_\lambda\rangle = P|\Psi_\lambda\rangle$ is the projection of the true eigenstate $|\Psi_\lambda\rangle$ onto the P space. Then we can solve Eq. (4) for $|\phi_\lambda\rangle$ as

$$H_{\rm BH}(E_\lambda)|\phi_\lambda\rangle = E_\lambda|\phi_\lambda\rangle, \quad \lambda = 1,\dots,D, \tag{5}$$

where we have introduced the following Bloch-Horowitz effective Hamiltonian $H_{\rm BH}$ defined purely in the P space,

$$H_{\rm BH}(E) = PHP - PVQ\frac{1}{E - QHQ}QVP. \tag{6}$$

Note that Eq. (5) requires a self-consistent solution, because $H_{\rm BH}(E_\lambda)$ depends on the eigenenergy E_λ. This is not a desirable property for the shell-model calculation, and therefore we adopt the energy-independent approach below.

C. Energy-independent approach

Next we introduce the energy-independent effective Hamiltonian in the P space. We first choose d eigenstates $\{|\Psi_i\rangle, i = 1,\dots,d\}$ among D solutions of Eq. (2), with $d \leqslant D$. Then we require that $|\phi_i\rangle = P|\Psi_i\rangle$, the P-space component of the chosen d eigenstates, be described by the d-dimensional effective Hamiltonian $H_{\rm eff}$ as

$$H_{\rm eff}|\phi_i\rangle = E_i|\phi_i\rangle, \quad i = 1,\dots,d. \tag{7}$$

The energy-independent effective Hamiltonian $H_{\rm eff}$ can be obtained by considering the following similarity

transformation of the Hamiltonian H:

$$\mathcal{H} = e^{-\omega} H e^{\omega}, \quad Q\omega P = \omega. \tag{8}$$

By construction, the transformed Hamiltonian, $\mathcal{H}$, gives the same eigenenergies as the original Hamiltonian H. The corresponding eigenstates $|\Psi_i\rangle$, however, are transformed into $e^{-\omega}|\Psi_i\rangle$. We require therefore that the second relation in Eq. (8), $Q\omega P = \omega$, satisfies $Pe^{-\omega}|\Psi_i\rangle = P(1-\omega)|\Psi_i\rangle = |\phi_i\rangle$; that is, the transformation does not change the P-space component $|\phi_i\rangle$ of the eigenstates.

Our next step includes the determination of ω. The most convenient way to determine ω is by using the equation

$$0 = Q\mathcal{H}P = QVP - \omega PHP + QHQ\omega - \omega PVQ\omega, \tag{9}$$

which decouples the P-space part in the transformed Schrödinger equation. This means that the P-space part of the transformed Hamiltonian, $P\mathcal{H}P$, is nothing but $H_{\rm eff}$ in Eq. (7). Then the effective Hamiltonian and the effective interaction can be written as

$$H_{\rm eff} = PHP + PVQ\omega, \quad V_{\rm eff} = PVP + PVQ\omega. \tag{10}$$

We note here that $H_{\rm eff}$ is energy independent. Furthermore, the derivation of $H_{\rm eff}$ requires the determination of ω to satisfy Eq. (9).

III. FORMAL THEORY OF EFFECTIVE INTERACTION

The decoupling equation (9), being nonlinear, can be solved by iterative methods to give $H_{\rm eff}$ and $V_{\rm eff}$ of Eq. (10). We first explain the KK method [17] for the degenerate model space and then turn to the EKK method [21,22] for the nondegenerate model space. Both methods eliminate the energy dependence of $H_{\rm BH}(E)$ of Eq. (6) by introducing the so-called $\hat{Q}$ box and its energy derivatives, resulting in an energy-independent effective interaction $H_{\rm eff}$.

A. Kuo-Krenciglowa method

In the KK method, we assume a degenerate model space, $PH_0P = \epsilon_0 P$. Then Eq. (9) reads

$$(\epsilon_0 - QHQ)\omega = QVP - \omega PVP - \omega PVQ\omega. \tag{11}$$

One way to solve this nonlinear equation is to write it in the following iterative form:

$$\omega^{(n)} = \frac{1}{\epsilon_0 - QHQ}\left(QVP - \omega^{(n)} V_{\rm eff}^{(n-1)}\right), \tag{12}$$

where $\omega^{(n)}$ and $V_{\rm eff}^{(n)} = PVP + PVQ\omega^{(n)}$ stand for ω and $V_{\rm eff}$ in the nth step, respectively. Then we immediately arrive at the following iterative formula for $V_{\rm eff}^{(n)}$,

$$V_{\rm eff}^{(n)} = \hat{Q}(\epsilon_0) + \sum_{k=1}^{\infty} \hat{Q}_k(\epsilon_0)\left\{V_{\rm eff}^{(n-1)}\right\}^k, \tag{13}$$

where we have defined $\hat{Q}$ box and its derivatives as follows:

$$\hat{Q}(E) = PVP + PVQ\frac{1}{E - QHQ}QVP,$$

$$\hat{Q}_k(E) = \frac{1}{k!}\frac{{\rm d}^k \hat{Q}(E)}{{\rm d}E^k}. \tag{14}$$

In the limit of $n \to \infty$, Eq. (13) gives $V_{\rm eff} = V_{\rm eff}^{(\infty)}$ if the iteration converges.

We stress here that the above KK method can only be applied, by construction, to a system with a degenerate unperturbed model space that satisfies $PH_0P = \epsilon_0 P$. It cannot be applied, for instance, to obtain the effective interaction for the model space composed of the sd shell and the pf shell.

B. Extended Kuo-Krenciglowa method

The EKK method is designed to construct an effective Hamiltonian $H_{\rm eff}$ for nondegenerate model spaces [21,22]. We first rewrite Eq. (9) as

$$(E - QHQ)\omega = QVP - \omega P\tilde{H}P - \omega PVQ\omega, \tag{15}$$

where

$$\tilde{H} = H - E \tag{16}$$

is a shifted Hamiltonian obtained by the introduction of the energy parameter E. Equation (15) plays the same role in the EKK method as Eq. (11) does in the KK method. By solving Eq. (15) iteratively as in the KK method, we obtain the following iterative scheme to calculate the effective Hamiltonian $H_{\rm eff}$,

$$\tilde{H}_{\rm eff}^{(n)} = \tilde{H}_{\rm BH}(E) + \sum_{k=1}^{\infty} \hat{Q}_k(E)\left\{\tilde{H}_{\rm eff}^{(n-1)}\right\}^k, \tag{17}$$

where

$$\tilde{H}_{\rm eff} = H_{\rm eff} - E, \quad \tilde{H}_{\rm BH}(E) = H_{\rm BH}(E) - E, \tag{18}$$

and $\tilde{H}_{\rm eff}^{(n)}$ stands for $\tilde{H}_{\rm eff}$ at the nth step. The effective Hamiltonian $H_{\rm eff}$ is obtained as $H_{\rm eff} = H_{\rm eff}^{(\infty)}$ and satisfies

$$\tilde{H}_{\rm eff} = \tilde{H}_{\rm BH}(E) + \sum_{k=1}^{\infty} \hat{Q}_k(E)\{\tilde{H}_{\rm eff}\}^k. \tag{19}$$

The effective interaction, $V_{\rm eff}$, is then calculated by Eq. (10) as $V_{\rm eff} = H_{\rm eff} - PH_0P$.

Let us now compare the EKK and the KK methods. First, and most importantly, the above EKK method does not require that the model space be degenerate. It can, therefore, be applied naturally to a valence space composed of several shells. Second, Eq. (17) changes $\tilde{H}_{\rm eff}$, while Eq. (13) changes only $V_{\rm eff}$ at each step of the iterative process. Third, to perform the iterative step of Eq. (17), we need to calculate $\hat{Q}_k(E)$ at the arbitrarily specified energy E, instead of at ϵ_0 for Eq. (13).

Equation (19) is interpreted as the Taylor series expansion of $\tilde{H}_{\rm eff}$ around $\tilde{H}_{\rm BH}(E)$, and changing E corresponds to shifting the origin of the expansion and, therefore, to a re-summation of the series. This explains why the left-hand side of Eq. (19) is independent of E, while each term on the right-hand side depends on E. This, in turn, means that we can tune the parameter E in Eq. (19) to accelerate the convergence of the series on the right-hand side, a feature that we exploit in actual calculations.

IV. MANY-BODY THEORY OF EFFECTIVE INTERACTION

For the purpose of obtaining the effective interaction for the shell model, we need to apply the formal theory of the effective interaction in Sec. III to nuclear many-body systems. In Sec. IV B, we explain the standard KK theory in a many-body system. Its diagrammatic expression can be established both in time-dependent [15] and time-independent [10] perturbation theory and is conveniently summarized by the $\hat{Q}$-box expansion in terms of the so-called folded diagrams [15]. In Sec. IV C, we show that $H_{\rm eff}$ in the EKK method has a similar expansion which can also be expressed by folded diagrams [15].

A. Model space in a many-body system

Our quantum many-body system is described by

$$H = H_0 + V = \sum \epsilon_\alpha a^\dagger_\alpha a_\alpha + \frac{1}{2}\sum V_{\alpha\beta,\gamma\delta} a^\dagger_\alpha a^\dagger_\beta a_\delta a_\gamma, \tag{20}$$

where H_0 is the unperturbed Hamiltonian and V is the two-body interaction. We limit ourselves, for the sake of simplicity, to two-body interactions only, although the theory can be extended to include three-body or more complicated nuclear forces.

In specifying single-particle states, we use indices a,b,c,d for valence single-particle states (active single-particle states) and p and h for passive particle and hole single-particle states, respectively. In a generic case, we use Greek indices.

In a many-body system, the P space is defined using the valence single-particle states that make up the P space. Let us take as an example the nucleus ^{18}O, where we treat ^{16}O as a closed-shell core. In this case we can define the P space by specifying the valence states to be determined by the single-particle states of the sd shell. The P space is then composed by the ^{16}O closed-shell core plus two neutrons in the sd shell.

In the following, we derive $H_{\rm eff}$ (and $V_{\rm eff}$) in Eq. (10) with the above Hamiltonian [Eq. (20)], which gives

$$H_{\rm eff}|\phi_i\rangle = E_i|\phi_i\rangle, \quad i = 1,\ldots,d, \tag{21}$$

for the many-body system.

B. Kuo-Krenciglowa method

Here we briefly explain the KK method in a degenerate P space. Many-body perturbation theory (MBPT) shows that the effective interaction, $V_{\rm eff}$, is conveniently written in terms of the so-called folded diagrams as [15]

$$V_{\rm eff} = \hat{Q}(\epsilon_0) - \hat{Q}'(\epsilon_0)\int \hat{Q}(\epsilon_0) + \hat{Q}'(\epsilon_0)\int \hat{Q}(\epsilon_0)\int \hat{Q}(\epsilon_0)\ldots, \tag{22}$$

where the integral sign represents the folding procedure, and $\hat{Q}'$ represents $\hat{Q}$-box contributions that have at least two NN interaction vertices. Note that, to have a degenerate P-space energy, ϵ_0, the single-particle energies in Eq. (20) for valence single-particle states, $\epsilon_a,\epsilon_b,\ldots$, are completely degenerate.

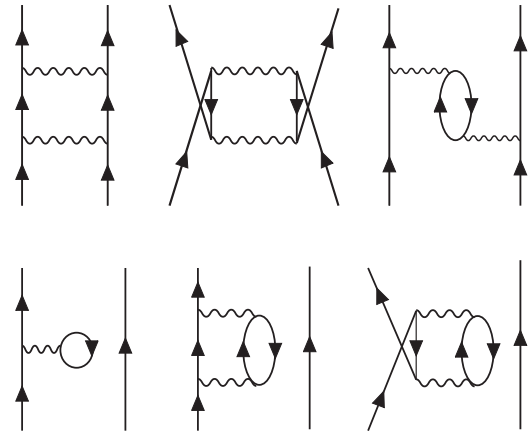

FIG. 1. Valence-linked $\hat{Q}$-box diagrams up to second order in V.

Equation (22) is the basis of the perturbative expansion of $V_{\rm eff}$ in the folded-diagram theory (see, for example, Ref. [15] for more details).

There are two points to be noted here. First, because we cannot evaluate the $\hat{Q}$ box defined in Eq. (14) exactly (which implies including all terms to infinite order), we use a perturbative expansion,

$$\hat{Q}(E) = PVP + PV\frac{Q}{E-H_0}VP + PV\frac{Q}{E-H_0}V\frac{Q}{E-H_0}VP + \cdots, \tag{23}$$

which we can currently evaluate up to the third order in the NN interaction. Second, the valence-linked diagram theorem states that we need to retain only the valence-linked part (see Fig. 1); i.e., unlinked parts can be proved to cancel among themselves [10,15]. At the same time, the eigenvalue E_i in Eq. (21) changes its meaning; it is no longer the total energy of the system, but is now the total energy measured from the true ground-state energy of the core.

In actual calculations, however, we do not calculate $V_{\rm eff}$ order by order using Eq. (22). Because the contribution of folded diagrams can be calculated by energy derivatives when the model space is degenerate [15], we can translate Eq. (22) into the following equation

$$V_{\rm eff} = \hat{Q}(\epsilon_0) + \sum_{k=1}^{\infty} \hat{Q}_k(\epsilon_0)\{V_{\rm eff}\}^k. \tag{24}$$

The above expression clearly shows that the iterative solution of Eq. (13) converges $V_{\rm eff}$ in the limit of $n \to \infty$.

We can summarize the KK method as follows: We calculate the valence-linked $\hat{Q}$-box diagrams (usually up to second or third order) and the corresponding energy derivatives at the degenerate P-space energy ϵ_0, and carry out the iteration of Eq. (13) starting from $V^{(0)}_{\rm eff} = V$. This procedure ultimately gives $V_{\rm eff} = V^{(\infty)}_{\rm eff}$.

At the end, we stress again that the above KK method can yield $V_{\rm eff}$ only for a degenerate model space. Suppose we are working with the harmonic oscillator shell model of ^{18}O, treating ^{16}O as the core. If we take the P space composed only

of the degenerate sd shell, the above KK method works well, as shown by many applications (see, for example, Ref. [16]). If, however, we take an enlarged P space defined by the nondegenerate sdf_7p_3 shell, the KK method breaks down. A naive calculation of $V_{\rm eff}$ by Eq. (22) easily leads to divergences of the $\hat{Q}$ box, as we see later.

C. Extended Kuo-Krenciglowa method

Here we derive the effective Hamiltonian $H_{\rm eff}$ of the EKK method, with an emphasis on its similarity with the KK method discussed above.

1. Derivation of the extended Kuo-Krenciglowa method

We consider first the general situation where the energies of the valence single-particle states in PH_0P are not necessarily degenerate. In this case, we have to apply the EKK formula Eq. (17) to our many-body systems.

We can easily confirm that, to derive Eq. (17), we need to change the decomposition Eq. (20) of the Hamiltonian in the KK method. Suppose we decompose the total Hamiltonian into an unperturbed Hamiltonian H_0' and the perturbation V',

$$\begin{aligned} H_0' &= PEP + QH_0Q, \\ V' &= V - P(E - H_0)P, \end{aligned} \tag{25}$$

or in the matrix form

$$H = H_0' + V' = \begin{pmatrix} E & 0 \\ 0 & QH_0Q \end{pmatrix} + \begin{pmatrix} P\tilde{H}P & PVQ \\ QVP & QVQ \end{pmatrix}, \tag{26}$$

where $\tilde{H} \equiv H - E$, and $H_0 = \sum \epsilon_\alpha a_\alpha^\dagger a_\alpha$. With the above unperturbed Hamiltonian H_0' in Eq. (25), we can treat the P space as being degenerate at the energy E, and therefore we can follow the derivation of Eq. (22) in the KK method, to achieve

$$\begin{aligned} \tilde{H}_{\rm eff} = \tilde{H}_{\rm BH}(E) - \hat{Q}'(E) \int \tilde{H}_{\rm BH}(E) \\ + \hat{Q}'(E) \int \tilde{H}_{\rm BH}(E) \int \tilde{H}_{\rm BH}(E) \cdots, \end{aligned} \tag{27}$$

which is then converted into

$$\tilde{H}_{\rm eff} = \tilde{H}_{\rm BH}(E) + \frac{{\rm d}\hat{Q}(E)}{{\rm d}E} \tilde{H}_{\rm eff} + \frac{1}{2!} \frac{{\rm d}^2\hat{Q}(E)}{{\rm d}E^2} \{\tilde{H}_{\rm eff}\}^2 + \cdots. \tag{28}$$

Note that Eqs. (27) and (28) are the EKK counterparts of Eqs. (22) and (24) of the KK method. We can solve Eq. (28) iteratively as done for Eq. (24).

Note that the above derivation of the EKK method is the same as that of the KK method apart from the decomposition of the Hamiltonian. Therefore, we need to retain only the valence-linked $\hat{Q}$-box diagrams in Eqs. (27) and (28), as we do for the KK method. To summarize, all that we have to know is, as in the KK method, the $\hat{Q}$ box and its energy derivatives, except that now it is defined at the parameter E.

2. Perturbative expansion of the $\hat{Q}$ box

We discuss here how one can accommodate the perturbative expansion of the $\hat{Q}$ box in the EKK formalism. For the sake of simplicity, we focus on a simple system composed of two particles on top of a closed-shell core in what follows, although the discussion is not restricted to this specific case. The projection operators P and Q are then given by

$$P = \sum_{a,b} a_a^\dagger a_b^\dagger |c\rangle\langle c| a_b a_a, \quad Q = 1 - P, \tag{29}$$

where $|c\rangle$ stands for the closed-shell core.

To become familiar with our new unperturbed Hamiltonian, H_0', we consider some selected examples; we show first the results from the operation of the new unperturbed Hamiltonian, H_0', on some selected many-particle states:

$$\begin{aligned} H_0' a_a^\dagger a_b^\dagger |c\rangle &= E a_a^\dagger a_b^\dagger |c\rangle, \\ H_0' a_a^\dagger a_p^\dagger |c\rangle &= (\epsilon_a + \epsilon_p) a_a^\dagger a_p^\dagger |c\rangle, \\ H_0' a_a^\dagger a_b^\dagger a_p^\dagger a_h |c\rangle &= (\epsilon_a + \epsilon_b + \epsilon_p - \epsilon_h) a_a^\dagger a_b^\dagger a_p^\dagger a_h |c\rangle. \end{aligned} \tag{30}$$

The first line is an example of a P-space state with two single-particle states on top of the closed-shell core, $|c\rangle$, while the second and third lines result in Q-space examples. The unperturbed energy of the P-space state $a_a^\dagger a_b^\dagger |c\rangle$ is E, while that of a Q-space state $a_a^\dagger a_p^\dagger |c\rangle$ results in $\epsilon_a + \epsilon_p$, a sum of unperturbed single-particle energies. It is important to get convinced that ϵ_a appears only in the Q-space energy, while $a_a^\dagger$ appears in all of the above three states.

In the perturbative expansion of $\hat{Q}(E)$ in Eq. (23), all the intermediate states are in the Q space, and their unperturbed energies are given as in the second and third lines of the above example. The general structure of $\hat{Q}(E)$ can then be given schematically by

$$\hat{Q}(E) = \prod \frac{V}{E - \left(\sum \epsilon_a + \sum \epsilon_p - \sum \epsilon_h\right)_{\rm int}}, \tag{31}$$

where the subscript "int" indicates intermediate states between two interaction vertices. Note that the parameter E appears in all the denominators in the EKK method.

Let us consider the $\hat{Q}$-box diagram shown in Fig. 2 as an example. The diagram is a contribution from the second-order

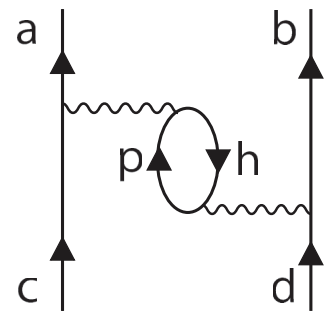

FIG. 2. Core-polarization diagram as a second order in V contribution to the $\hat{Q}$ box.

term in Eq. (23), and gives the following contribution to $\hat{Q}(E)$:

$$\text{Fig.2(EKK)} \rightarrow \frac{V_{ah,cp}V_{pb,hd}}{E-\epsilon_c-\epsilon_b-\epsilon_p+\epsilon_h}. \quad (32)$$

However, if we employ the KK method to calculate the contribution to $\hat{Q}(\epsilon_0)$ from Fig. 2, we would get

$$\text{Fig. 2(KK)} \rightarrow \frac{V_{ah,cp}V_{pb,hd}}{(\epsilon_c+\epsilon_d)-\epsilon_c-\epsilon_p+\epsilon_h-\epsilon_b} = \frac{V_{ah,cp}V_{pb,hd}}{-\epsilon_p+\epsilon_h}, \quad (33)$$

where, in going to the second line, we have used the fact that the P space is degenerate, and therefore $\epsilon_a=\epsilon_b=\epsilon_c=\epsilon_d$ and $\epsilon_c+\epsilon_d=\epsilon_0$.

Two points should be noted from the above example. First, in a degenerate model space, the EKK result Eq. (32) with $E=\epsilon_0$ coincides with the KK result Eq. (33). This is a direct consequence of the fact that the EKK formula contains the KK formula as a special case. Second, we can see the problem of divergence of the KK formula applied naively to a nondegenerate model space. Consider the case of ^{18}O as an example, and let the P space consist of two major shells ($1s0d$ and $1p0f$ shells). Then, the denominator of the first line in Eq. (33) vanishes for $b,c,p \in 1s0d$ shell, $a,d \in 1p0f$ shell, and $h \in 0p$ shell, leading thereby to a divergence. The above mechanism is just one of many examples which show that we really need to use the EKK formalism to derive effective interactions for model spaces consisting of several shells.

3. The energy parameter E

Here we make several points in connection with the new parameter E in the EKK theory.

First, by virtue of the arbitrariness of the parameter E, we can get around the problems of the poles of the $\hat{Q}$ box. As explained with the example in Fig. 2, the $\hat{Q}$-box contribution [Eq. (33)] is divergent in the KK formula when we work in a nondegenerate model space. However, the EKK counterpart [Eq. (32)] becomes divergent only for specific values of E. This means that we can always select a parameter E that makes the $\hat{Q}$ box behave smoothly as a function of E.

Second, the parameter E provides us with a reasonable test of the calculation. Equation (19) shows that the resulting effective Hamiltonian H_{eff} does not depend on the value of E, provided that we have the exact $\hat{Q}$ box in Eq. (19). Any approximation may spoil the E independence of H_{eff} and thereby of other physical quantities described by H_{eff}. This may, in turn, imply that a $\hat{Q}$ box that gives E-independent physical quantities is a good approximation to the exact $\hat{Q}$ box. In the most sophisticated calculations to date, we can evaluate the $\hat{Q}$-box diagrams only up to third order in the perturbation V at most, and we can include only a limited number of excitations in the intermediate states (typically including up to 10–20 oscillator quanta excitations), because of practical computational limitations. In Sec. V, we present numerical tests of the above E independence.

Here we explain how to fix the value of E in the actual calculations. If there are no intruder states in the target states $\{|\phi_i\rangle, i=1,\ldots,d\}$ that are to be described by H_{eff}, it can be shown that there is a finite range of E values that make the series in Eq. (28) convergent [22]. The convergence is usually at its fastest when E is fixed around the mean value of the target energies $\{E_i, i=1,\ldots,d\}$. Let us come back to our specific case of two particles on top of a core, and employ a single-particle basis of the harmonic oscillator. Let $\epsilon_a^{\min}$ be the minimum energy of active (valence) particle states. We then expect that our target states are distributed around $E \sim 2\epsilon_a^{\min}$, which serve as the first guess for E. It is also clear that the lowest energy of the Q-space states is $2\epsilon_a^{\min}+1\hbar\omega$, which gives the lowest position of the poles of $\hat{Q}(E)$.

In actual calculations, the allowed range of E, which is limited both from above and from below, can be estimated as follows. Let us increase E from the above "*optimal*" value $2\epsilon_a^{\min}$. As E approaches the lowest pole $2\epsilon_a^{\min}+1\hbar\omega$ of $\hat{Q}(E)$, $\hat{Q}(E)$ and its derivatives in Eq. (28) would diverge. However, if we choose too low a value of $E \ll 2\epsilon_a^{\min}$, the resultant energy denominators in the $\hat{Q}(E)$ would be dominated by E, but not by the unperturbed energies of the intermediate states. In this situation, we have to expect that our approximation, truncation of the intermediate states at some unperturbed energies, cannot be justified.

In the next section, we present numerical examples where E is varied in some range around $E \sim 2\epsilon_a^{\min}$.

V. NUMERICAL RESULTS

To apply the EKK formalism to nuclear systems, we consider simple nuclei composed of two nucleons on top of a given closed-shell core, ^{18}O,^{18}F and ^{42}Ca,^{42}Sc, employing a single-particle basis defined by the harmonic oscillator unperturbed Hamiltonian. As the P space for ^{18}O and ^{18}F, we employ the sd shell (degenerate case) and the sdf_7p_3 shell (nondegenerate case) composed of the sd shell and the $0f_{7/2}$ and the $1p_{3/2}$ single-particle states. The P space for ^{42}Ca,^{42}Sc is the pf shell (degenerate case), and the pfg_9 shell (nondegenerate case) composed of all the pf-shell single-particle states and the $0g_{9/2}$ single-particle state. In the degenerate P space, both the KK and the EKK methods can be used, while in the nondegenerate P space only the EKK method is applicable.

Our input interaction V in the Hamiltonian Eq. (20) is the low-momentum interaction $V_{\text{low}k}$ with a sharp cutoff $\Lambda = 2.5$ fm^{-1}, derived from the chiral χN^{3}LO interaction of Entem and Machleidt [23,24]. Our total $(P+Q)$ Hilbert space is composed of the harmonic oscillator basis states in the lowest nine major shells. The Q-space degrees of freedom come into play either by the KK method or the EKK method through the $\hat{Q}$ box that is calculated to third order in the interaction V. The final effective interactions are thus obtained in the P space of one or two major shells.

We ought to mention two points. First, the amount of oscillator quanta excitations in each term in perturbation theory, may not be fully adequate if one is interested in final shell-model energies that are converged with respect to the number of intermediate excitations in the $\hat{Q}$-box diagrams; see the discussions of Vary *et al.* and Sommermann *et al.* [25,26]. In the present work we have included all possible intermediate

excitations which can be formed within nine major shells. This means that for a second-order contribution like the core-polarization diagram of Fig. 2, we can have at most (depending on symmetries) excitations of 8 oscillator quanta. Typically, to get fully converged low-lying energy levels of different nuclei, one needs from 6 to 12 oscillator quanta excitations. Second, neglected many-body correlations, like those arising from three-body forces are not taken into account. Such effects, together with other many-body correlations not included here are expected to play important roles; see, for example, the recent studies of neutron-rich oxygen and calcium isotopes [27–31]. However, the aim here is to study the effective interactions that arise from the KK and the EKK methods in one and two major shells. Detailed calculations for nuclei along various isotopic chains will be presented elsewhere.

In the actual calculation of the $\hat{Q}$ box using the harmonic oscillator basis functions, we drop the Hartree-Fock diagram contributions, assuming that it is well simulated by the harmonic oscillator potential, as in many of the former works [16].

To show how the EKK method works, we present separate studies of (i) the two-body matrix elements (TBMEs) of the effective interaction $V_{\rm eff}$ and (ii) several energy levels obtained by shell model calculations. In particular, we focus on the E independence of the numerical results; as discussed in Sec. II, the effective Hamiltonian $H_{\rm eff}$ obtained with the exact $\hat{Q}$ box is independent on the energy parameter E, and so are physical quantities calculated with $H_{\rm eff}$. In other words, the explicit E dependence of the first term $H_{\rm BH}(E)$ [or equivalently $\hat{Q}(E)$] in Eq. (28) is canceled by other terms that represent the folded-diagram contributions, making thereby $H_{\rm eff}$ (and therefore $V_{\rm eff}$) energy independent. In actual calculations, however, we can calculate the $\hat{Q}$ box only up to third order in V, and we have to examine the E dependence of the right-hand side of Eq. (19). In what follows, we see clearly that the $\hat{Q}$ box up to third order is sufficient to achieve an almost E-independent effective interaction $V_{\rm eff}$ (or $H_{\rm eff}$).

A. EKK method in *sd* shell and sdf_7p_3 shell

In this section, we consider ^{18}O and ^{18}F as two-nucleon systems on top of the ^{16}O closed-shell core. We calculate the effective interactions $V_{\rm eff}$ in the degenerate sd shell and in the nondegenerate sdf_7p_3-shell model spaces. The input of the EKK method is the $\hat{Q}$ box calculated up to third order in V with the harmonic oscillator basis of $\hbar\omega = 14$ MeV. We set the origin of the energy as $\epsilon_{sd} = 0$, which suggests that the optimal choice of E is $E \sim 0$.

1. Degenerate sd-shell model space

In Fig. 3, we show our numerical results for the TBMEs and level energies calculated in the degenerate sd-shell model space for the neutron-neutron channel (^{18}O) and in Fig. 4 the proton-neutron channel (^{18}F).

To see the E independence of the numerical results for $V_{\rm eff}$, calculations are performed for several values of E. As explained before, the optimal value of E may be estimated as $E \sim 2\epsilon_{sd} = 0$. Note also that $E = 0$ is far from the lowest pole

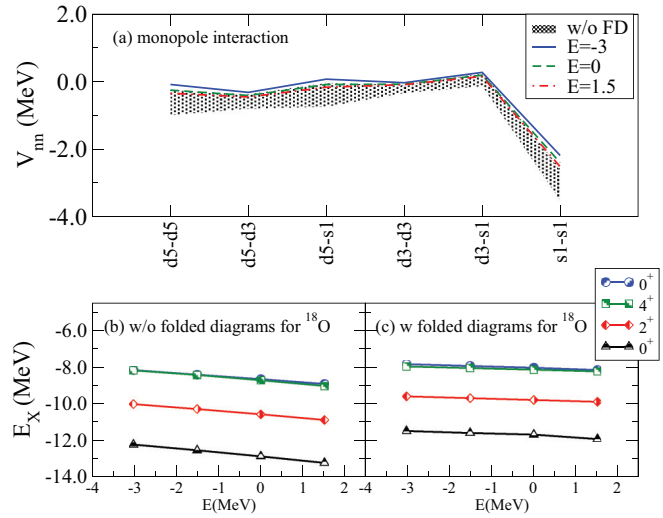

FIG. 3. (Color online) E dependence of the EKK results of neutron-neutron channel in the sd shell (degenerate model space). The figure shows the monopole part of $V_{\rm eff}$ (denoted by V_{nn}) [see Eq. (34)] and the level energies of ^{18}O with respect to ^{16}O. In panel (a), the monopole panel, dotted lines (which make the shaded area) show the results without the folded-diagram contributions for $-3 \leqslant E \leqslant 1.5$ MeV. The solid line, dashed line, and dot-dashed line show the V_{nn} for $E = -3, 0, 1.5$ MeV, respectively. In panels (b) and (c), energy levels are calculated for $E = -3, -1.5, 0, 1.5$ MeV (b) without and (c) with the folded-diagram contribution. Triangles, diamonds, squares, and circles show the energy levels of the ground and the first, second, and third excited states, respectively.

of $\hat{Q}(E)$, $E = E^{\rm min}_{\rm pole} = 1\hbar\omega = 14$ MeV and the calculation is free from the divergence problem of the $\hat{Q}$ box. We have thus varied E in the range of $-3 \leqslant E \leqslant 1.5$ MeV in Figs. 3 and 4.

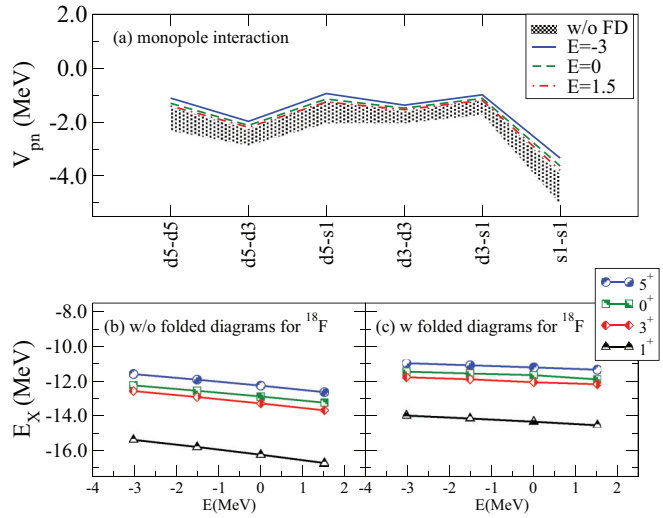

FIG. 4. (Color online) E dependence of the EKK results of proton-neutron channel in the sd shell (degenerate model space). (a) Monopole part of the interaction and (b) level energies of ^{18}F without folded diagrams and (c) with folded diagrams. We use the same notation as in Fig. 3.

Obviously, the EKK method with $E = 0$ coincides exactly with the KK method because our P space is degenerate now [compare Eqs. (32) and (33)].

To study the effect on the various matrix elements, we analyze the monopole term in the neutron-neutron channel in Fig. 3(a). The monopole part of $V_{\rm eff}$, is defined as

$$V_{\rm eff}{}^{T}_{j,j'} = \frac{\sum_J (2J+1)\langle jj'|V_{\rm eff}|jj'\rangle_{JT}}{\sum_J (2J+1)}. \qquad (34)$$

Let us look at the dotted lines (which make a shaded band in the figure) that are calculated by dropping the folded-diagram contributions, i.e., by replacing $V_{\rm eff}$ simply with $\hat{Q}(E)$. We can see clearly that $\hat{Q}(E)$ depends strongly on E. Next, let us turn to the EKK results that include all the folded-diagram contributions in the right-hand side of Eq. (28). They are shown by solid lines for $E = -3, 0, 1.5$ MeV, whose difference can hardly be seen. The above observation suggests that the folded diagrams cancel the E dependence of $\hat{Q}(E)$ and yield an almost E-independent $\tilde{H}_{\rm eff}$ (and $V_{\rm eff}$) in Eq. (28).

In panels (b) and (c) of Fig. 3, we show several energy levels of ^{18}O with respect to ^{16}O obtained by shell-model calculations with our effective interaction $V_{\rm eff}$. Here the single-particle energies in the shell-model diagonalization are taken from the USD interaction [1,32]; the single-particle energies of the states (in the isospin formalism) $\epsilon_{d_{5/2}}$, $\epsilon_{s_{1/2}}$, and $\epsilon_{d_{3/2}}$ are -3.9478, -3.1635, and 1.6466 MeV, respectively.

Panels (b) and (c) show the results without and with folded-diagram contributions, respectively. We note that in panel (b) the energy levels are decreasing functions of E, which is explained by the E dependence of $\hat{Q}(E)$. However, in panel (c), we see that the energy levels are almost independent of the parameter E, as they should be.

The above observation also implies that the evaluation of the $\hat{Q}$ box up to third order in V is sufficient to establish a seemingly E independence of the right-hand side of Eq. (28) and therefore of $V_{\rm eff}$ on the left-hand side.

Figure 4 shows the results for $V_{\rm eff}$ in the proton-neutron channel and level energies for ^{18}F with the same setting as for ^{18}O. We can repeat exactly the same arguments as we did for ^{18}O and realize that the folded-diagram contribution eliminates the E dependence, to a large extent, of $\hat{Q}(E)$ to give, almost, an E-independent $V_{\rm eff}$ and energy levels.

2. *Nondegenerate sdf_7p_3 shell*

Here we examine ^{18}O and ^{18}F in the nondegenerate P space, labeled the sdf_7p_3 shell here, composed of the sd shell and the $0f_{7/2}$ and $1p_{3/2}$ single-particle states. In this nondegenerate model space, the standard KK method cannot be applied, because it leads to divergences, as discussed above. The EKK method offers, however, a viable approach to this system. To date, therefore, there have been only empirical interactions in this model space; see, for example, the effective interaction employed in Ref. [33].

Figures 5 and 6 show the numerical results of the EKK method in the sdf_7p_3 model space, in the same way as Figs. 3 and 4 for the degenerate sd shell. In what follows, we introduce the wording "intershell interaction" for the interaction between particles in different major shells; for example, we can have one particle in the sd shell and the other one in the pf shell. Similarly, we use "intrashell interaction" for interactions between particles within a single major shell.

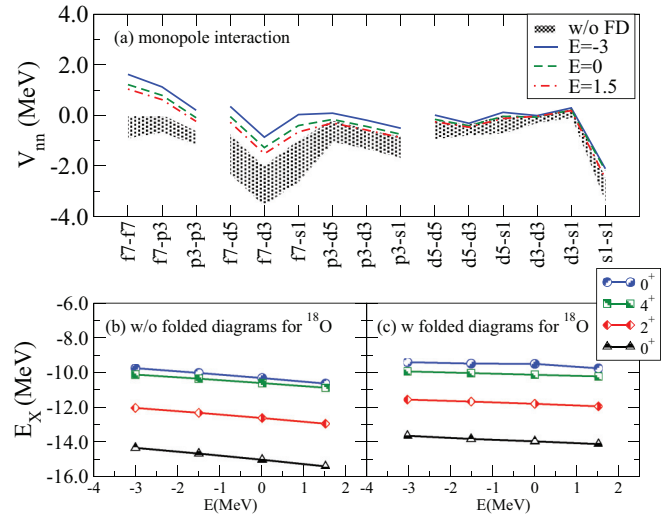

FIG. 5. (Color online) E dependence of the EKK results of neutron-neutron channel in the sdf_7p_3 shell (nondegenerate model space). (a) Monopole part of the interaction and (b) level energies of ^{18}O without folded diagrams and (c) with folded diagrams. We use the same notation as in Fig. 3.

Let us first study the monopole part of the TBMEs of $V_{\rm eff}$ [Fig. 5(a) for neutron-neutron channel and Fig. 6(a) for proton-neutron channel]. Here we have intershell interactions in addition to the intrashell interactions within the sd shell and within the pf shell. We see that the intershell interactions depend more strongly on E without the folded diagrams than the intrashell interaction within the sd shell. This feature is attributable to the fact that $\hat{Q}(E)$ for the intershell interaction

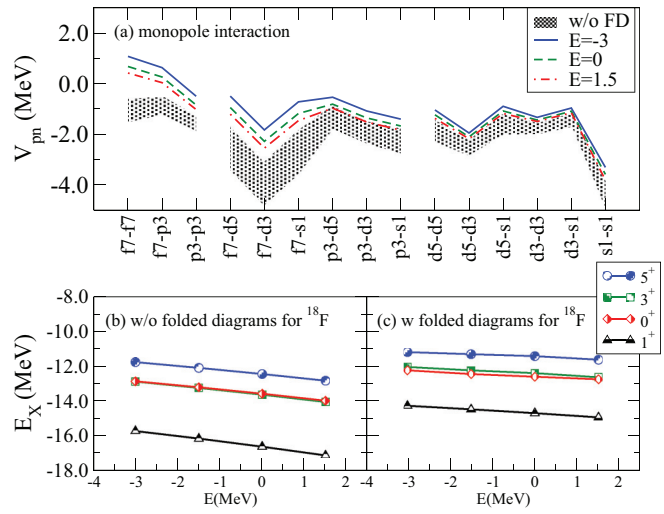

FIG. 6. (Color online) E dependence of the EKK results of proton-neutron channel in the sdf_7p_3 shell (nondegenerate model space). (a) Monopole part of the interaction and (b) level energies of ^{18}F without folded diagrams and (c) with folded diagrams. We use the same notation as in Fig. 4.

has intermediate states with small energy denominators. This figure clearly shows that the folded-diagram contributions soften the strong E dependence of the $\hat{Q}(E)$, and the resulting $V_{\rm eff}$ becomes almost independent of E, indicating that the EKK method may represent a stable and useful approach to the nondegenerate case as well, here the sdf_7p_3 shell.

From the panels of the energy levels of ^{18}O and ^{18}F, we can draw the same conclusion for the degenerate sd shell; the folded-diagram contribution to energy levels that depend weakly on the parameter E.

3. Comparison of KK and EKK methods

The main advantage of our EKK method is that it allows for a consistent treatment of the nondegenerate model space. However, in the KK method, the naive perturbative calculation of the $\hat{Q}$ box in Eq. (22) leads to divergence in the nondegenerate sdf_7p_3 shell, as discussed in Sec. IV C.

One possible *ad hoc* way to avoid this divergence is to artificially force the sdf_7p_3 shell to be degenerate in energy by shifting the single-particle energies [28]. Although there is no physical justification for this artificial shift, it removes the poles that arise in the various $\hat{Q}$ box diagrams.

Note, however, that the obtained $V_{\rm eff}$ is defined with artificially degenerate single-particle energies. Furthermore, in actual calculations, this method dose not necessarily lead to a convergent result even with all the folded diagrams in Eq. (22).

For the purpose of comparing the EKK method with the *ad hoc* treatment of the nondegeneracy in the KK method, we apply the EKK method to both sets of unperturbed Hamiltonians: one with the artificially degenerate sdf_7p_3 shell and the other with the nondegenerate sdf_7p_3 shell. Note that the EKK method in the artificially degenerate sdf_7p_3 shell simulates the *ad hoc* KK method explained above. In this calculation, to obtain convergence, we set $E = -1.5$ MeV in both cases.

Figure 7 shows the monopole part of the effective interaction $V_{\rm eff}$ in the sdf_7p_3 shell interaction for the neutron-neutron channel. The dashed lines show the results with the *ad hoc* modification of the unperturbed Hamiltonian, as explained above. The solid lines display the results in the nondegenerate model space. To show the contribution of the $\hat{Q}$ box and folded diagrams, we display also the monopole part of the first-order term of the $\hat{Q}$ box. This term is energy independent.

It is interesting to note that the intershell (pf-sd) interaction and the intrashell (sd-sd) interaction are more attractive in the EKK method than in the *ad hoc* KK method. This discrepancy clearly comes from the difference in the energy denominator in the $\hat{Q}$ box. Suppose we have two particles within $f_{7/2}$ or $p_{3/2}$ states. The magnitude of the energy denominator shown in Eq. (31) is larger, making thereby the $\hat{Q}$ box smaller in the EKK method than in the *ad hoc* KK method. For the intershell (pf-sd) interaction and the intrashell (sd-sd) interaction, this difference makes the interaction for the artificially degenerate single-particle states more repulsive. However, in the intrashell (pf-pf) interaction, the EKK results are more repulsive than the *ad hoc* KK results. This can be understood as follows; the effect of the folded-diagram contribution is quite large in the

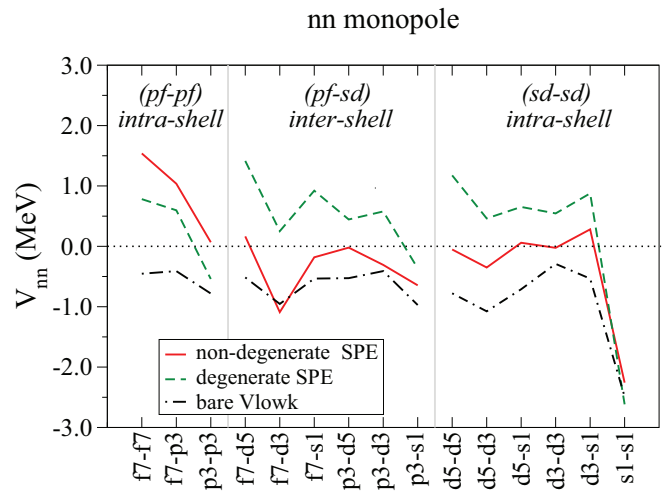

FIG. 7. (Color online) Plot of the monopole part of $V_{\rm eff}$ defined by the sdf_7p_3 model space. The effective interaction has been constructed using nondegenerate single-particle energies (solid lines) and the *ad hoc* degenerate single-particle energies (dashed lines); see text for further details. Both calculations are performed in the neutron-neutron channel. We include also the monopole part that arises from the effective interaction to first order in perturbation theory (dash-dotted lines). The latter interaction is energy independent by construction.

EKK method because we use $P\tilde{H}P$ in the folding procedure instead of PVP. This difference makes the contribution of the folded diagrams larger.

The above comparison shows that there is a sizable difference between the effective interaction in the EKK method and in the *ad hoc* KK method, and the difference affects mostly the intershell interaction.

B. EKK method in pf shell and pfg_9 shell

We apply the EKK method to the nuclei ^{42}Ca and ^{42}Sc as well. These nuclei can be described as two nucleons on top of a ^{40}Ca core. Here the degenerate model space is composed of the single-particle states of the pf shell, while our nondegenerate model space is defined by the single-particle states of the pf shell and the single-particle state $g_{09/2}$. We have performed the calculation in the same way as in Sec. V A 2, but with an oscillator parameter $\hbar\omega = 11$ MeV, which is appropriate for the ^{40}Ca region. We have taken $\epsilon_{pf} = 0$ and therefore our first guess for the energy parameter is $E = 0$.

1. Results for pf shell

Figures 8 and 9 show the effective interaction $V_{\rm eff}$ defined in the degenerate pf shell. In Fig. 8, panel (a) shows the neutron-neutron monopole interactions and panels (b) and (c) display the energy levels of ^{42}Ca. Figure 9 shows the results for ^{42}Sc, the proton-neutron channel, in the same manner. In the shell-model diagonalization, the single-particle energies are taken from the GXPF1 interaction [2]; the particle energies (in the isospin formalism) of $\epsilon_{f_{7/2}}$, $\epsilon_{p_{3/2}}$, $\epsilon_{p_{1/2}}$, and $\epsilon_{f_{5/2}}$ are equal to -8.6240, -5.6793, -4.1370, and -1.3829 MeV, respectively.

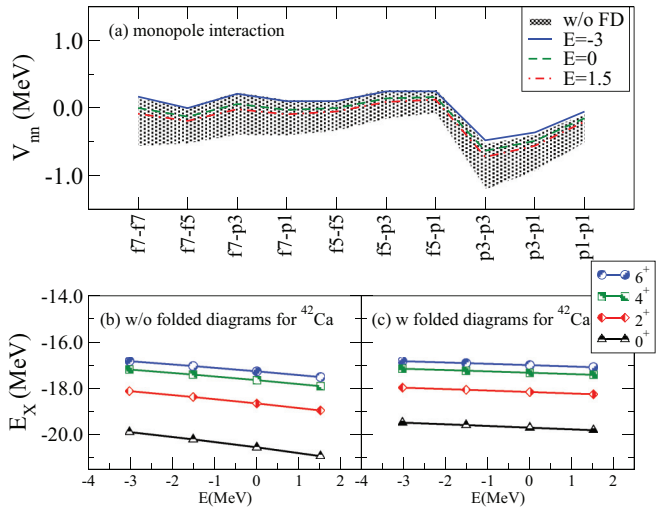

FIG. 8. (Color online) E dependence of the EKK results of neutron-neutron channel in the pf shell (degenerate model space). (a) Monopole part of the interaction and (b) level energies of ^{42}Ca without folded diagrams and (c) with folded diagrams. We use the same notation as in Fig. 3.

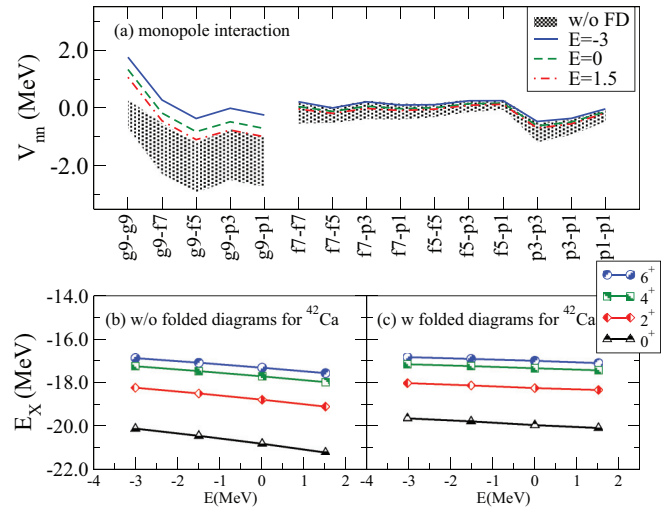

FIG. 10. (Color online) E dependence of the EKK results of neutron-neutron channel in the pfg_9 shell (nondegenerate model space). (a) Monopole part of the interaction and (b) level energies of ^{42}Ca without folded diagrams and (c) with folded diagrams. We use the same notation as in Fig. 3.

We have carried out the calculation by varying E in the range of $-3 \leqslant E \leqslant 1.5$ MeV. Clearly, we can make the same observation as in Sec. V A 1; the shaded bands in the monopole panels shrink when we include folded diagrams, resulting in a monopole part of $V_{\rm eff}$ almost independent (or weakly dependent) of E. Moreover, from the energy levels of ^{42}Ca [Figs. 8(b) and 8(c)] and ^{42}Sc [Figs. 9(b) and 9(c)], we observe that the folded diagrams result in a weak dependence on the parameter E for the lowest-lying levels.

2. Results for pfg_9 shell

As our final example, we present the results for the pfg_9 shell in Fig. 10 for the neutron-neutron channel and Fig. 11 for the proton-neutron channel. The parameter E is varied in the range of $-3 \leqslant E \leqslant 1.5$ MeV. The particle energies (in the isospin formalism) of $\epsilon_{f_{7/2}}$, $\epsilon_{p_{3/2}}$, $\epsilon_{p_{1/2}}$, $\epsilon_{f_{5/2}}$ and $\epsilon_{g_{9/2}}$ are equal to -8.6240, -5.6793, -4.1370, -1.3829, and 2.1000 MeV, respectively. We note again the role played by folded diagrams; they result in a weak E dependence of the $\hat{Q}(E)$, yielding an almost E-independent effective interaction $V_{\rm eff}$ and energy

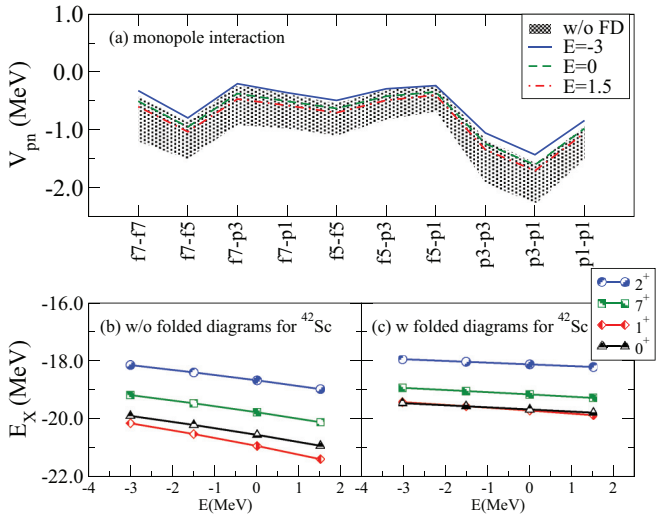

FIG. 9. (Color online) E dependence of the EKK results for the proton-neutron channel in the pf shell (degenerate model space). (a) Monopole part of the interaction and (b) energy levels of ^{42}Sc without folded diagrams and (c) with folded diagrams. We use the same notation as in Fig. 4.

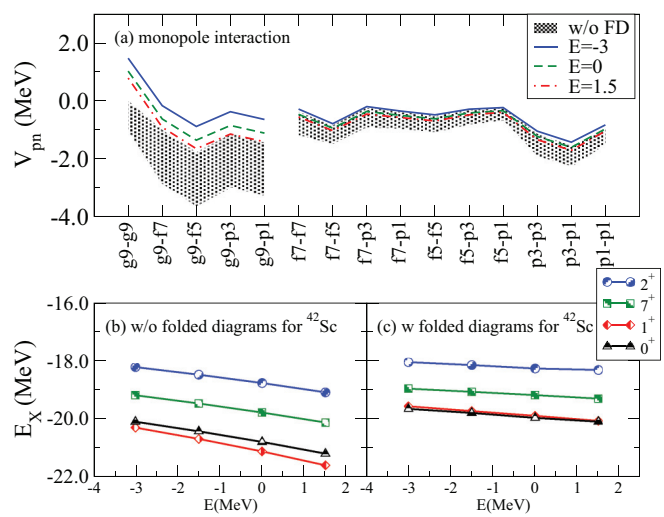

FIG. 11. (Color online) E dependence of the EKK results for the proton-neutron channel in the pfg_9 shell (nondegenerate model space). (a) Monopole part of the interaction and (b) energy levels of ^{42}Sc without folded diagrams and (c) with folded diagrams. We use the same notation as in Fig. 4.

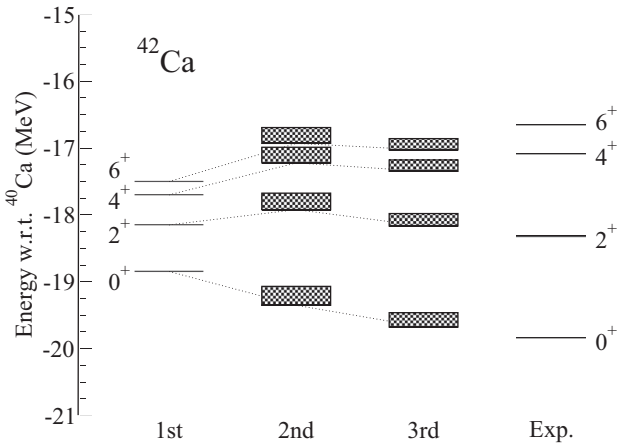

FIG. 12. Energy levels of the ground state and low-lying states of ^{42}Ca using the $\hat{Q}$ box to first, second, and third order in the interaction. The rightmost levels represent the experimental values. Energies are measured from the closed-shell core, ^{40}Ca. The TBMEs (neutron-neutron channel) are obtained by the EKK method, with the parameter E in the range $-3 \leqslant E \leqslant 0$ MeV. The shaded bands indicate the variation of calculated energy levels for $-3 \leqslant E \leqslant 0$ MeV.

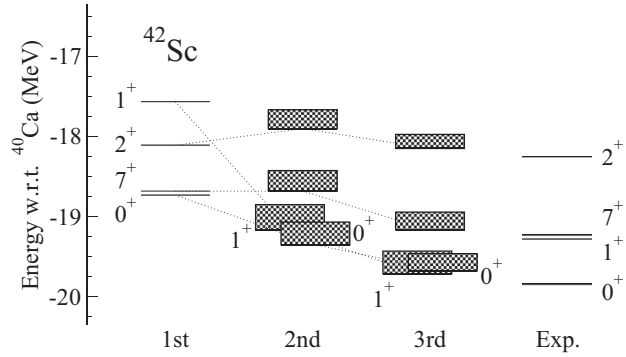

FIG. 13. Energy levels of the ground state and low-lying states of ^{42}Sc with respect to ^{40}Ca core. The TBMEs (proton-neutron channel) are obtained with the EKK method with the parameter $-3 \leqslant E \leqslant 0$ MeV. Because we do not include Coulomb effects throughout the calculation, the absolute values are shifted by -7.2 MeV, so that the 0^+ state forms the $T = 1$ triplet state with the corresponding 0^+ ground state of ^{42}Ca. Other notation is the same as in Fig. 12.

levels of ^{42}Ca [see Figs. 10(b) and 10(c)] and ^{42}Sc [see Figs. 11(b) and 11(c)].

C. Application of the EKK method to shell-model calculations

With effective Hamiltonians derived by the EKK method, we can study the role of such Hamiltonians in actual shell-model calculations. Here we focus on the previously discussed systems, with at most two valence nucleons outside a closed-shell core. Results from large-scale shell-model calculations will be presented elsewhere.

For this purpose, Fig. 12 shows the low-lying energy levels for ^{42}Ca obtained by the shell-model calculation with the same setting as in Sec. V B 1. The TBMEs are derived by the EKK method, with the $\hat{Q}$ box calculated to first, second, and third order in the interaction V. The parameter E is varied in the range of $-3 \leqslant E \leqslant 0$ MeV in the calculation of the second-order and the third-order $\hat{Q}$ box. Note that the first-order $\hat{Q}$ box is V itself and is independent of E. The leftmost levels show the result with the first-order $\hat{Q}$ box. The middle two levels represent the results with the second-order and third-order $\hat{Q}$ box, where the shaded bands show the range of the energy levels corresponding to $-3 \leqslant E \leqslant 0$ MeV. The rightmost levels are the experimental data.

As discussed above, by construction, all the physical results are independent of E if our $\hat{Q}$ box is calculated without any approximation. In other words, the weaker dependence on E implies a better approximation to the $\hat{Q}$ box (see Figs. 3–6 and 8–11). This means that the width of the shaded band may be taken as a measure of the size of the error.

In Fig. 12, independently of the comparison to experiment, two types of convergence can be seen: The first one is (i) the convergence of the energy levels with respect to the order of the perturbation, and the second one is (ii) the convergence of the bandwidths (E dependence of the energy levels) with respect to the order of the perturbation.

Let us start with discussions on convergence issue (i). Figure 12 shows that the magnitude of the third-order contribution is approximately 30% as large as that of the second-order contribution. A simple estimate from these observations tells us that the perturbation series make a geometric series with common ratio $\sim$0.3. We can then expect that the fourth-order correction to the $\hat{Q}$ box is small.

Let us turn to convergence case (ii). Figure 12 exhibits also that, compared with the second-order $\hat{Q}$ box, the bandwidths are smaller for the third-order $\hat{Q}$ box, as we would expect. Besides these theoretical features, the agreement with experiment is acceptable.

Next we examine the proton-neutron channel using ^{42}Sc as our test case. The results are shown in Fig. 13. The experimental values (right-most levels) are shifted by -7.2 MeV so that the 0^+ state forms the $T = 1$ triplet state with corresponding 0^+ ground state of ^{42}Ca, because we presently do not take into account any isospin dependence of the nuclear force or the Coulomb interaction.

Here we observe similar patterns to those seen in the neutron-neutron channel of Fig. 12. However, we notice that as far as convergence case (i) is concerned, the contribution of third-order terms is not necessarily smaller than second-order contributions.

However, for convergence case (ii), we observe smaller bandwidths for the third-order $\hat{Q}$ box results as compared with those obtained with the second-order $\hat{Q}$ box. This may indicate that the third-order $\hat{Q}$ box represents a better approximation than the second-order $\hat{Q}$ box.

The agreement with experimental data is rather nice for the $0^+, 7^+$, and 3^+ states, but we observe a slight overbinding for the 1^+ state. From the convergence property of the 1^+ state, it is unlikely that fourth-order contributions to the $\hat{Q}$ box could play an important role. Several explanations for this discrepancy are possible. One possibility for this overbinding is that the single-particle energies presently used are not fully adequate.

As mentioned above, we have employed the single-particle energies determined from the GXPF1 [2] interaction. These energies are the results of a fit together with the two-body interaction to reproduce experimental data. The experimental data that enter the fitting procedure consist of selected observables from pf-shell nuclei. Because the GXPF1 interaction differs from those derived here, other sets of single-particle energies could have been more appropriate. Another possibility is that our Q space and order in perturbation theory may not be large enough. Thus, there may be missing many-body correlations which could play an important role. Three-body forces [27–31] are examples of many-body contributions not studied here. However, the aim of this work has been to study the recently developed EKK formalism for deriving effective interactions for more than one major shell. The role of more complicated many-body correlations will be the focus of future works.

VI. CONCLUSION

We have presented a novel many-body theory (the so-called EKK method) to calculate the effective interaction $V_{\rm eff}$ for the shell-model calculation that is applicable not only to degenerate model spaces, but also to nondegenerate model spaces. The method is based on a reinterpretation of the unperturbed Hamiltonian and the interacting part. The final expressions for the effective interactions can be understood as a Taylor series expansion of the Bloch-Horowitz Hamiltonian around a newly introduced parameter E. Because the change in E should not affect the effective interactions $V_{\rm eff}$, the E independence of the numerical results provides us with a sensible test of our framework and the approximations we make in the actual calculations.

In this work, we have presented numerical results for the effective two-body NN interactions $V_{\rm eff}$, with applications to shell-model calculations of selected nuclei, with and without the contribution from the folded diagrams. The degenerate model spaces are the sd shell for the nuclei ^{18}O and ^{18}F and the pf shell for the nuclei ^{42}Ca and ^{42}Sc. Our nondegenerate model spaces consist of the single-particle states from the sdf_7p_3 shell and the pfg_9 shell. Based on our numerical results, we have found that our method works well in practical situations. For degenerate model spaces, our method gives the same results as the conventional KK method. In the nondegenerate model space, which is beyond the applicability of the KK method, we have shown that our method works nicely.

Second, we have shown that our $V_{\rm eff}$ (including $\hat{Q}$-box diagrams up to third order and folded diagrams to infinite order) and therefore the energy levels are almost independent of the parameter E. This, in turn, may suggest that the perturbative expansion of the $\hat{Q}$ box through third order gives almost converged results. For limited model spaces, however, as observed in the Introduction as well, the presence of so-called intruder states [19,20] may lead to the divergence of the order-by-order perturbative expansion of the effective interaction. In particular, a low-lying state like the 0_2^+ state of ^{18}O is assumed to be a four-particle-two-hole excitation, implying thereby the need for a larger model space. It is therefore not certain that the seemingly good convergence and almost energy-independent effective interaction may hold for higher orders in the perturbative expansion. However, the advantage of the EKK method is that it allows for a consistent calculation of effective interactions for larger shell-model spaces. This may alleviate some of the above convergence issues.

Third, the difference between the EKK method and the KK method with an *ad hoc* modification of the unperturbed Hamiltonian is significant, especially for intershell interactions. This can have a large impact, for example, on the investigation of neutron-rich nuclei where the degrees of freedom defined by two or more major oscillator shells are important.

Finally, we stress that our method has established a robust way to calculate microscopically the effective interaction in nondegenerate model spaces. These spaces involve typically more than one major oscillator shell. We believe that this is an indispensable step to make the nuclear shell model a reliable theory, in particular for exotic nuclei, based on a microscopic effective interaction derived from the realistic NN interactions.

ACKNOWLEDGMENTS

We thank Gaute Hagen and Koshiroh Tsukiyama for fruitful discussions. We are grateful to Prof. N. Shimizu for his invaluable help for our computations. This work is supported in part by a Grant-in-Aid for Scientific Research (A) No. 20244022 and also by a Grant-in-Aid by JSPS (Grant No. 228635), by the JSPS Core to Core program "International Research Network for Exotic Femto Systems" (EFES), the CNS-RIKEN joint research project on large-scale nuclear-structure calculations, and the high-performance computing project NOTUR in Norway. This work was supported by the Research Council of Norway under Contract No. ISP-Fysikk/216699.

[1] B. A. Brown, W. A. Richter, R. E. Julies, and B. H. Wildenthal, Ann. Phys. **182**, 191 (1988).
[2] M. Honma, T. Otsuka, B. A. Brown, and T. Mizusaki, Phys. Rev. C **65**, 061301 (2002).
[3] Y. Utsuno, T. Otsuka, T. Glasmacher, T. Mizusaki, and M. Honma, Phys. Rev. C **70**, 044307 (2004).
[4] A. Poves and A. Zuker, Phys. Rep. **70**, 235 (1981).
[5] A. Poves, J. Sánchez-Solano, E. Caurier, and F. Nowacki, Nucl. Phys. A **694**, 157 (2001).
[6] P. Navrátil, S. Quaglioni, I. Stetcu, and B. R. Barrett, J. Phys. G **36**, 083101 (2009).
[7] B. R. Barrett, P. Navrátil, and J. P. Vary, Prog. Part. Nucl. Phys. **69**, 131 (2013).
[8] E. D. Jurgenson, P. Maris, R. J. Furnstahl, P. Navrátil, W. E. Ormand, and J. P. Vary, Phys. Rev. C **87**, 054312 (2013).
[9] C. Bloch, Nucl. Phys. **6**, 329 (1958).
[10] B. Brandow, Rev. Mod. Phys. **39**, 771 (1967).
[11] P. J. Ellis and E. Osnes, Rev. Mod. Phys. **49**, 777 (1977).
[12] J. Morrison and I. Lindgren, *Atomic Many-body Theory* (Springer, Berlin, 1982).
[13] D. Klein, J. Chem. Phys. **61**, 786 (1974).

[14] K. Suzuki, Prog. Theor. Phys. **68**, 246 (1982).
[15] T. T. S. Kuo and E. Osnes, *Folded-Diagram Theory of the Effective Interaction in Nuclei, Atoms and Molecules*, Lecture Notes in Physics Vol. 364 (Springer, Berlin, 1990).
[16] M. Hjorth-Jensen, T. T. S. Kuo, and E. Osnes, Phys. Rep. **261**, 125 (1995).
[17] E. M. Krenciglowa and T. T. S. Kuo, Nucl. Phys. A **235**, 171 (1974).
[18] K. Suzuki and S. Y. Lee, Prog. Theor. Phys. **64**, 2091 (1980).
[19] T. H. Schucan and H. A. Weidenmüller, Ann. Phys. **73**, 108 (1972); **76**, 483 (1973).
[20] P. Schaefer, Ann. Phys. **87**, 375 (1974).
[21] K. Takayanagi, Nucl. Phys. A **852**, 61 (2011).
[22] K. Takayanagi, Nucl. Phys. A **864**, 91 (2011).
[23] D. R. Entem and R. Machleidt, Phys. Rev. C **68**, 041001(R) (2003).
[24] R. Machleidt and D. R. Entem, Phys. Rep. **503**, 1 (2011).
[25] J. P. Vary, P. D. Sauer, and C. W. Wong, Phys. Rev. C **7**, 1776 (1973).
[26] H. M. Sommermann, H. Müther, K. C. Tam, T. T. S. Kuo, and A. Faessler, Phys. Rev. C **23**, 1765 (1981).
[27] T. Otsuka, T. Suzuki, J. D. Holt, A. Schwenk, and Y. Akaishi, Phys. Rev. Lett. **105**, 032501 (2010).
[28] J. D. Holt, T. Otsuka, A. Schwenk, and T. Suzuki, J. Phys. G **39**, 085111 (2012).
[29] T. Otsuka and T. Suzuki, Few-Body Syst. **54**, 891 (2013).
[30] G. Hagen, M. Hjorth-Jensen, G. R. Jansen, R. Machleidt, and T. Papenbrock, Phys. Rev. Lett. **108**, 242501 (2012).
[31] G. Hagen, M. Hjorth-Jensen, G. R. Jansen, R. Machleidt, and T. Papenbrock, Phys. Rev. Lett. **109**, 032502 (2012).
[32] B. A. Brown and B. H. Wildenthal, Annu. Rev. Nucl. Part. Sci. **38**, 29 (1988).
[33] Y. Utsuno, T. Otsuka, T. Mizusaki, and M. Honma, Phys. Rev. C **60**, 054315 (1999).